Eur Biophys J (1999) 28: 222–234

ARTICLE

Olivier Thoumine · Olivier Cardoso
Jean-Jacques Meister

Changes in the mechanical properties of fibroblasts during spreading: a micromanipulation study

Received: 22 June 1998 / Revised version: 14 October 1998 / Accepted: 15 October 1998

Abstract Cell morphology is controlled in part by physical forces. If the main mechanical properties of cells have been identified and quantitated, the question remains of how the cell structure specifically contributes to these properties. In this context, we addressed the issue of whether cell rheology was altered during cell spreading, taken as a fundamental morphological change. On the experimental side, we used a novel dual micromanipulation system. Individual chick fibroblasts were allowed to spread for varying amounts of time on glass microplates, then their free extremity was aspirated into a micropipet at given pressure levels. Control experiments were also done on suspended cells. On the theoretical side, the cell was modeled as a fluid drop of viscosity μ, bounded by a contractile cortex whose tension above a resting value was taken to be linearly dependent on surface area expansion. The pipet negative pressure was first adjusted to an equilibrium value, corresponding to formation of a static hemispherical cap into the pipet. This allowed computation, through Laplace's law, of the resting tension (τ_0), on the order of 3×10^{-4} N/m. No difference in τ_0 was found between the different groups of cells studied (suspended, adherent for 5 min, spread for 0.5 h, and spread for 3 h). However, τ_0 was significantly decreased upon treatment of fibroblasts with inhibitors of actin polymerization or myosin function. Then, the pressure was set at 30 mmH_2O above the equilibrium pressure. All cells showed a biphasic behavior: (1) a rapid initial entrance corresponding to an increase in surface area, which was used to extract an area expansion elastic modulus (K), in the range of 10^{-2} N/m; this coefficient was found to increase up to 40% with cell spreading; (2) a more progressive penetration into the pipet, linear with time; this phase, attributed to viscous behavior of the cytoplasm, was used to compute the apparent viscosity (μ, in the range of $2–5\times10^4$ Pa s) which was found to increase by as much as twofold with cell spreading. In some experiments the basal force at the cell-microplate interface was quantitated with flexible microplates and found to be around 1 nN, in agreement with values calculated from the model. Taken together, our results indicate a stiffening of fibroblasts upon spreading, possibly correlated with structural organization of the cytoskeleton during this process. This study may help understand better the morphology of fibroblasts and their mechanical role in connective tissue integrity.

Key words Cell morphometry · Cortical tension · Area expansion modulus · Apparent viscosity · Microplate

O. Thoumine (✉) · J.-J. Meister
Biomedical Engineering Laboratory,
Swiss Federal Institute of Technology,
CH-1015 Lausanne, Switzerland
e-mail: olivier.thoumine@epfl.ch

O. Cardoso
Laboratoire de Physique Statistique, Ecole Normale Supérieure,
24 Rue Lhomond, F-75231 Paris Cedex 05, France

Introduction

Cellular deformations, e.g. those occurring during locomotion, are essential to numerous physiological and pathological situations. For example, following a wound, fibroblasts migrate into the injured area and participate in the repair process, in particular by pulling on extracellular matrix fibers (James and Taylor 1969; Stopak and Harris 1982; Harris 1988). Although powered by chemical reactions, changes in cell shape are mechanical processes controlled by physical forces (Elson 1988; Lauffenburger and Horwitz 1996). To better understand these processes, various mechanical tests have been carried out on cells, in particular with micromanipulation techniques. These include aspiration into micropipets (Evans and Yeung 1989), imposition of forces using glass microneedles (Kolega 1986; Dennerll et al. 1989; Felder and Elson 1990) or microplates (Thoumine and Ott 1997 a), poking the cell surface (Petersen et al. 1982), twisting ferromagnetic particles by magnetometry (Valberg and Albertini 1985; Wang et al. 1993), or pulling on surface-attached microspheres with optical tweezers (Kucik et al. 1991; Choquet et al. 1997).

Such experiments have led to the understanding that cellular morphology is determined by two antagonistic processes (Chicurel et al. 1998): (1) active force generation

through conversion of chemical energy, and (2) passive resistance of the cell and extracellular structure. In the first category are protrusive forces arising from polymerization of cytoskeletal elements (Peskin et al. 1993; Dogterom and Yurke 1997), which for exemple drive lamellipodium extension in fibroblasts (Cramer et al. 1994) or axon initiation in neurons (Zheng et al. 1993). Contractile forces, in particular those expressed at cell-substrate contacts (Ingber 1991; Sims et al. 1992; Thoumine and Ott 1996) or at the cell cortex (Albrecht-Buehler 1987; Tran-Son-Tay et al. 1991), which mainly rely on the actin-myosin motor, also belong to the first group. In the second category are all mechanical processes that resist these active forces, for example the intracellular pressure build-up due to cortex tension (Yanai et al. 1996), the extracellular matrix or substrate resistance to cytoskeletal traction (Schiro et al. 1991; Wang et al. 1993), and the viscoelastic strength of the overall cell structure (cytoplasm, membranes, and cytoskeleton).

One question that remains open, however, is how cellular organization controls rheology. In other words, what alterations in mechanical properties accompany changes in cell morphology and structure? To start answering these questions, one may look closer at a fundamental morphological change, namely cell spreading. Spreading of cells onto a surface is a dynamic process occurring on a time scale of several minutes to hours (Evans 1988; Bereiter-Hahn et al. 1990; Dunn and Zicha 1995), depending in particular on substrate adhesiveness and temperature. During this process, cells progressively switch from a spherical to a flattened morphology. This is accompanied by structural changes at the cytoskeletal and adhesive levels (Soranno and Bell 1982; David-Pfeuty 1985; Mooney et al. 1995). Although spreading is a common phenomenon in routine cell culture and in vivo (e.g. following cytokinesis), deep physical understanding of this process is lacking. Also, there is a need for an accurate quantification of the physically relevant parameters in cell spreading, in particular cortical tension, area elasticity, and adhesive energy (Evans 1995), to push early theoretical models (Bardsley and Aplin 1983) a step further. Such a physical approach may lead to a better interpretation of the biological events underlying cell spreading.

In this context, our study aimed at evaluating changes in cell mechanical properties during the course of cell spreading. A dual micromanipulation system was used, in which the upper surface of fibroblasts spreading on a glass microplate was aspirated into a micropipet. A theoretical analysis of the experiments, based on continuum mechanics, allowed calculation of fibroblast cortical tension, surface elasticity, and apparent viscosity from morphometric and pressure measurements.

Materials and methods

Cell culture

Fibroblasts were isolated from the hearts of 10-day-old chick embryos as described previously (Thoumine and Ott 1996). Cells were cultured in minimal essential medium (MEM) supplemented with 0.05% gentamycin, 2 mM L-glutamine, and 10% fetal bovine serum (FBS), and used at passages 3–6. Cell culture reagents were purchased from Seromed (Germany).

Microinstrument preparation

Microplates (Thoumine and Ott 1997a) were fabricated from 0.1×1×100 mm borosilicate bars (VitroCom, Mountain Lakes, N.J., USA) using a micropipet puller (Sutter Instrument, Novato, Calif., USA). Two types of microplates were made, by adjusting the parameters of the puller: *rigid* ones (stiffness, taken as the force divided by the deflection of the tip, was greater than 10^{-7} N/μm), and *flexible* ones (stiffness around 10^{-9} N/μm). Tip dimensions were about 3×30 μm for rigid microplates, and 1×10 μm for flexibles ones. Micropipets were pulled from glass capillaries (Clark Electromedical Instruments, Pangbourne, UK) with outer and inner diameters of 1.0 and 0.8 mm, respectively) using the same micropipet puller. A microforge (Narishige, Japan) was used to break the tips of micropipets in a straight fashion and bend the pipets to 90°.

Micromanipulation set-up

The manipulation system consists of an Axiovert 135 inverted microscope (Zeiss, Oberkochen, Germany) placed on an anti-vibration table (TMC, Peabody, Mass., USA). Microinstruments are fixed to steel arms and maneuvered using two 30-mm mechanical micromanipulators (Physik Instrumente, Waldbronn, Germany), mounted on each side of the microscope stage. One of the translator axes is controlled by a piezoelectric element with a 25 μm range, allowing for precise final adjustment of the microinstrument position. Cells are manipulated in a lab-made chamber (30 mm in diameter, 3 mm deep), which can be displaced horizontally on the microscope stage. Sequences of cell deformation under bright-field illumination were recorded using a 40×/0.75 objective, a 1.6× Optovar lens, and a CCD camera (Cohu, San Diego, Calif., USA) connected to a time-lapse video cassette recorder (Sanyo, Japan). Prior to manipulation, the observation chamber was filled with culture medium containing 20 mM Hepes. One pipet was filled with the same solution and positioned in the chamber using the micromanipulator on the left side. The pipet was connected to a pressure control system comprising a 10-ml reservoir filled with culture medium and two reservoirs filled with water (Sato et al. 1987; Thoumine and Ott 1997b). Rack-and-pinion control over the last reservoir elevation allowed pressure head adjustment over a 200-mm range, with a resolution of 0.5 mmH_2O. Zero pressure was set by examining the movement of 1 μm latex microspheres (Molecular Probes, Poortgebouw, The Netherlands) added to the solution. Pressure was monitored using a transducer (Cole Palmer, Vernon Hills, Ill., USA) connected to the pressure line.

Control of cell spreading

The medium was replaced by MEM containing 20 mM Hepes (MEM-Hepes). Cells from a 1 cm^2 culture well were detached using 0.005% trypsin-20 mM EGTA in McCoy's 5 a medium lacking Ca^{2+}, resuspended in MEM-Hepes, and added to the chamber. A trypsin concentration as low as possible was used to minimize effects on cell surface properties, but still produce cell detachment in reasonable times. Using the micromanipulator on the right, several fibroblasts were captured on a rigid microplate, as described (Thoumine and Ott 1997 a). Cells adhered well to bare glass in the absence of FBS. After 5 min, the medium was replaced by MEM-Hepes containing 10% FBS, and cells were either tested directly (cells in this condition are referred to as *adherent*) or transferred in a CO_2 incubator at 37 °C for a time period of 0.5 h or 3 h (cells in these conditions are referred to as *spread-0.5 h* and *spread-3 h*, respectively). For transfer, the extremity of the arm carrying the microplate was fixed onto the chamber with a custom-made system, and the whole assembly was placed in the incubator. At the end of the incubation period, cells were brought back to the microscope and subjected to mechanical testing. Control experiments were carried out on non-adherent fibroblasts, which were aspirated either directly after detachment (*suspended-control*) or maintained in suspension for 3 h at 37 °C before aspiration (*suspended-3 h*). In some cases, fibroblasts were resuspended in medium containing 0.3 μg/ml cytochalasin D (*suspended-cyt D*), or 20 mM 2,3-butanedione monoxime (*suspended-BDM*). These drugs were obtained commercially (Sigma, St Louis, Mo., USA).

Mechanical test

For adherent and spread fibroblasts, the microplate carrying the cells was turned by a 90° angle to visualize the cells from the side, and the upper surface of one cell was placed to the contact of the micropipet tip, using piezoelectric positioning (Fig. 1). Negative pressure was increased by increments of 2.5 mmH_2O, until formation of a static hemispherical cap inside the pipet was observed (Evans and Yeung 1989). Negative pressure was then quickly raised by 30 mmH_2O above this equilibrium value, and maintained constant for 10 min. Finally, pressure was set back to the equilibrium value for another 5 min. Suspended cells were manipulated as described previously (Thoumine and Ott 1997 b) and exposed to the same aspiration test. There was no adhesion of cells to the micropipet because serum was present in the medium. Mechanical tests were kept short compared to the time course of spreading, to avoid interference with basic properties acquired during spreading. All experiments were performed at room temperature. In some tests on suspended and adherent cells, the equilibrium aspiration pressure was determined for various pipet diameters (3–8 μm).

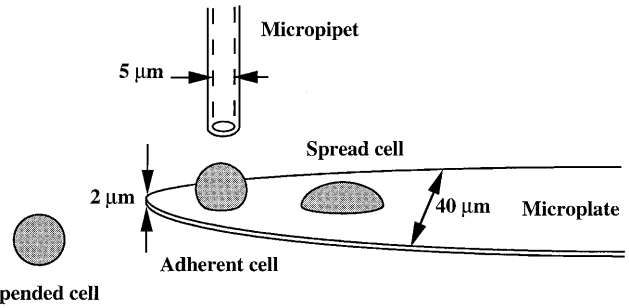

Fig. 1 Schematic drawing of the microplate-micropipet experiment. The three categories of cells (suspended, adherent, and spread) are shown

Image acquisition and analysis

Videotapes were played back and one image every 30 s was digitized with a personal computer (Power Macintosh, Apple) equipped with a frame grabber card (Scion, Frederick, Md., USA). Using an image analysis software (NIH Image, v1.60), we measured the following parameters (Fig. 2): (1) the pipet internal radius (R_p); (2) the length of the aspirated portion (L); (3) for adherent cells, the diameter of the contact zone between the cell and the microplate ($D_a = 2R_a$); (4) for suspended cells, the cell radius outside the pipet (R_c); (5) the angle between the normal to the micropipet axis and the tangent to the cell contour at the pipet mouth (θ_p); (6) the angle between the plane of the microplate and the tangent to the cell contour at the interface (θ_a). The error on length measurements was about 0.3 μm. We also estimated the total surface area and volume of the cells from 2D images, by building a specific function within the software. Each shape was cut into three segments: (1) the hemispherical cap, (2) the cylindrical part in the pipet, and (3) the portion of cell outside the pipet. Each segment was modeled as a Bézier curve which was then discretized in small layers. The 3D shape was reconstructed from theses layers, assuming an axisymmetry around a local axis situated in the middle of the layer. This supplemented version of NIH Image is available upon request or from the Internet.[1]

Measurement of the basal force

In some experiments, cells were captured on flexible microplates, and let adhere for 5 min. Cells were then exposed to the same aspiration test described above. The deflection of the microplate was followed over time dur-

[1] Note: Public domain program, developed at the US National Institute of Health and available by anonymous ftp from zippy.nimh.nih.gov or on floppy disk from the National Technical Information Service, Springfield, VA, USA, part number PB95-500195GEI. Both adapted source code and compiled application for MacOS are available at http://www.lps.ens.fr/~cardoso/NIH/NIH.html

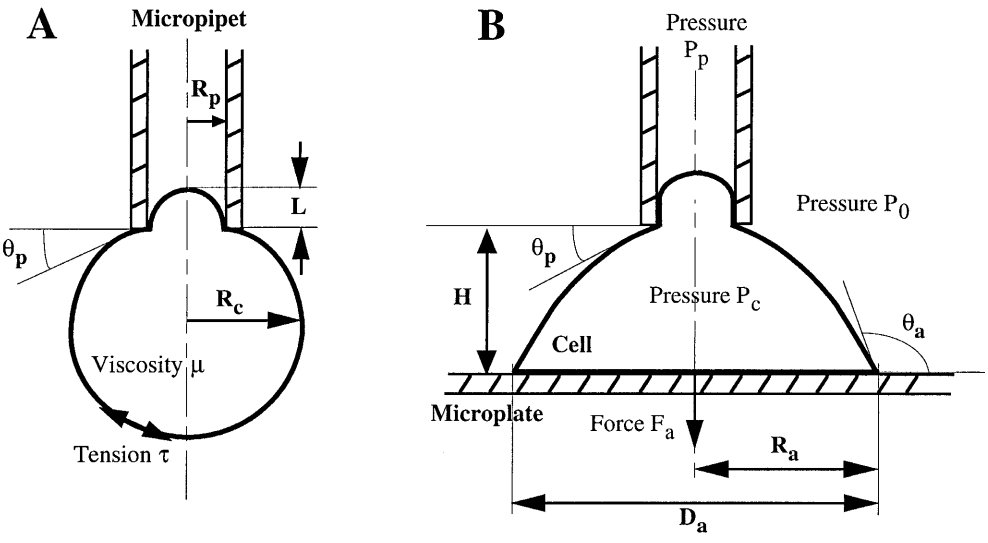

Fig. 2 Schematic diagram showing the morphometric and mechanical parameters for a suspended cell **(A)**, and a cell spreading on a microplate (**B**)

ing aspiration. To calibrate the force, cells were allowed to relax for 10 min at the end of the test. Then, negative pressure was increased sequentially by increments of 10 mmH_2O (up to 60 mmH_2O), and the pipet was displaced at a speed of about 2 μm/s. At a certain point during pulling, corresponding to a given deflection of the flexible microplate, cells slipped out of the pipet: the force at the basal surface (microplate stiffness times deflection) was then equal to the force at the apical side (pressure times pipet cross section). The relationship between the measured deflection and the apical force was linear, the slope of which being taken as the microplate stiffness (0.90 ± 0.55 nN/μm, $n = 11$). The force during aspiration was obtained by multiplying the measured deflection by this stiffness. We estimate the error on the force to be about 15%.

Actin and nucleus staining

In some cases, fibroblasts adherent to a microplate or aspirated into a micropipet were stained for F-actin, using rhodamine-phalloidin as a marker. Fixing, permeabilization, and staining were carried out directly in the chamber, following an established protocol (Thoumine and Ott 1996). In other experiments, cell nuclei were stained with syto 13 (3 μM in culture medium for 0.5 h), then fibroblasts were detached and aspirated. Both fluorophores were from Molecular Probes. Cells were observed by epifluorescence illumination using a 63×/1.25 oil objective and appropriate filter sets.

Theoretical analysis

Model hypotheses and parameters

Fibroblasts were modeled as fluid drops bounded by a cortex under persistent tension, and possessing area elasticity. The model is borrowed from existing descriptions of leukocyte rheology (Evans and Yeung 1989; Yeung and Evans 1989; Tran-Son-Tay et al. 1991; Needham and Hochmuth 1992), whose main hypotheses seem to also hold for fiboblasts. Indeed, tension is a critical feature of fibroblasts (Albrecht-Buehler 1987; Galbraith and Sheetz 1997; Thoumine and Ott 1997a), and generally attributed to an actin-rich peripheral layer; it contributes to the adoption of a spherical shape upon detachment with trypsin. Here, we suppose fibroblast cortical tension to be 2D isotropic, with a resting value τ_0. Surface elasticity in fibroblasts has been demonstrated by several studies (Felder and Elson 1990; Lo et al. 1998). We describe it by an area expansion modulus K (N/m), adopting a first-order elastic law for the cortical tension (Needham and Hochmuth 1992):

$$\tau = \tau_0 + K\,\alpha \qquad (1)$$

where $\alpha = (A - A_0)/A_0$ is the relative change in surface area (A is the cell area in the deformed state, and A_0 is the area in the relaxed state). Fibroblasts also have viscous properties, especially dominant at times scales of minutes (Thoumine and Ott 1997a). To model this behavior, we approximate the cytoplasm as a spherical core made of a Newtonian fluid with a high viscosity, μ. We further hypothesize that fibroblasts possess, as leukocytes (Simon and Schmid-Schönbein 1988; Evans and Yeung 1989), a large excess in plasma membrane area. This is in agreement with electron microscopy images showing numerous folds on the surface of suspended fibroblasts, which are almost absent from spread cells (Vasiliev 1985; O'Neill et al. 1986). Thus, increases in apparent (or cortical) area can easily be accomodated by unfolding of membrane wrinkles (Yeung and Evans 1989).

Adhesion and spreading

Adhesion corresponds to the formation of a planar contact between the cell and the substrate. The hypothesis of isotropic tension predicts that the region outside the contact zone should have a spherical shape. Thus, the morphology

of adherent fibroblasts may be described by a truncated sphere, whose volume is $V = \pi H^2 (R - H/3)$, where H is the height and R is the radius of the sphere. Elementary geometry gives two relationships between H, R, the contact angle θ_a, and the contact diameter D_a: $\cos\ \theta_a = H/R - 1$, and $D_a = 2R \sin\ \theta_a$. Under the further assumption that cell volume is conserved during adhesion and spreading, then $V = 4\pi R_0^3/3$, where R_0 is the radius of the suspended cell. From these equations, one obtains the following relationships between H, D_a, and θ_a:

$$(H/R_0)^3 = 4/[3/(1+\cos\ \theta_a) - 1] \quad (2)$$

$$(D_a/2R_0)^3 = 4\sin\theta_a(1-\cos\theta_a)/[(1+\cos\theta_a)\ (2-\cos\theta_a)] \quad (3)$$

and

$$D_a = 2[(8R_0^3/H - H^2)/3]^{1/2} \quad (4)$$

Aspiration: equilibrium analysis

When the aspiration pressure is adjusted so that the cell forms a hemispherical cap in the pipet, there exists a mechanical equilibrium. For a suspended cell (Fig. 2A), the persistent cortical tension at equilibrium, τ_{eq}, can be related to the aspiration pressure by applying Laplace's law at the pipet entrance and at the equatorial section (Evans and Yeung 1989):

$$\Delta P_{eq} = 2\ \tau_{eq}(1/R_p - 1/R_c) \quad (5)$$

where ΔP_{eq} is the difference between the pressure in the external medium (P_0) and the pressure in the pipet (P_p) at equilibrium, R_p the pipet radius, and R_c the radius of the cell outside the pipet, which is sligthly lower than R_0 (Fig. 2). For an adherent cell (Fig. 2B), one can write two equations for the cortex (Evans et al. 1980; Evans and Leung 1984; Tözeren et al. 1992).

1. For the hemispherical cap inside the pipet:

$$2\pi R_p \tau_{eq} = \pi R_p^2 (P_c - P_p) \quad (6)$$

2. For the region between the pipet and the plate:

$$2\pi R_p \tau_{eq} \sin\theta_p = 2\pi R_a \tau_{eq} \sin\theta_a - \pi(R_a^2 - R_p^2)\ (P_c - P_0) \quad (7)$$

where P_c is the cell internal pressure (unknown). By eliminating P_c from Eqs. (6) and (7), one obtains, for $R_a \neq R_p$:

$$\Delta P_{eq} = 2\tau_{eq}[1/R_p - (R_a \sin\theta_a - R_p \sin\theta_p)/(R_a^2 - R_p^2)] \quad (8)$$

In the limit of $R_a \to 0$ (case of a non-adherent cell), Eq. (8) becomes:

$$\Delta P_{eq} = 2\tau_{eq}(1/R_p - \sin\theta_p/R_p) \quad (9)$$

which is equivalent to Eq. (5), since $\sin\theta_p = R_p/R_c$ for a suspended cell (Fig. 2A).

Aspiration: rapid entry phase

When the aspiration pressure is adjusted above the equilibrium value, the model predicts a rapid jump due to cortex elasticity, followed by a steady entry due to viscous flow of the cytoplasm. We hypothesize a pseudo-equilibrium during the initial entry phase (neglecting viscous dissipation which occurs on a longer time scale), so that the instantaneous tension τ is related to the transient aspiration pressure ΔP through an equation similar to Eq. (8):

$$\Delta P = 2\tau[1/R_p - (R_a \sin\theta_a - R_p \sin\theta_p)/(R_a^2 - R_p^2)] \quad (10)$$

Combining with Eqs. (1) and (8), ΔP_{exc} being the aspiration pressure in excess of the equilibrium value ($\Delta P_{exc} = \Delta P - \Delta P_{eq}$), we obtain the relationship:

$$\Delta P_{exc} = 2K\ \alpha[1/R_p - (R_a \sin\theta_a - R_p \sin\theta_p)/(R_a^2 - R_p^2)] \quad (11)$$

Aspiration: flow into the pipet

In the case of a suspended cell, the internal viscosity μ can be expressed as a function of the rate of entry (dL/dt), the excess pressure (ΔP_{exc}), the pipet and cell radii, and a parameter η which represents the ratio of viscous dissipation in the cortex versus that in the fluid core (Yeung and Evans 1989); η was demonstrated to be about 0.01 for leukocytes (Evans and Yeung 1989). A linearized version, taking $\eta = 0.01$, gives (Needham and Hochmuth 1992; Zhelev and Hochmuth 1994):

$$\mu = \Delta P_{exc}/[6\ dL/dt\ (1/R_p - 1/R_c)] \quad (12)$$

In the case of adherent and spread cells, we simply replaced the scaling term $(1/R_p - 1/R_c)$ in Eq. (5) by the one in Eq. (8), and arrived at the following equation:

$$\mu = \Delta P_{exc}/\{6\,dL/dt[1/R_p - (R_a \sin\theta_a - R_p \sin\theta_p)/(R_a^2 - R_p^2)]\} \quad (13)$$

Force at the basal surface

At equilibrium, the force F_a at the cell-microplate interface is (Fig. 2B):

$$F_a = 2\pi R_a \tau_{eq} \sin\theta_a - \pi R_a^2 (P_c - P_0) \quad (14)$$

Combining with Eqs. (6) and (7), one obtains:

$$F_a = \pi \Delta P_{eq}(\sin\theta_a/R_a - \sin\theta_p/R_p)/\{(1/R_p^2 - 1/R_a^2) \cdot [1/R_p - (R_a \sin\theta_a - R_p \sin\theta_p)/(R_a^2 - R_p^2)]\} \quad (15)$$

By approximation, we use the same relation for the non-equilibrium phase.

Results

Morphology of fibroblasts on microplates

We first quantitatively examined the degree of cell spreading. Chick fibroblasts adhered well to untreated borosilicate microplates, but failed to spread on them at room temperature, even in the presence of serum (Fig. 3A, C). To

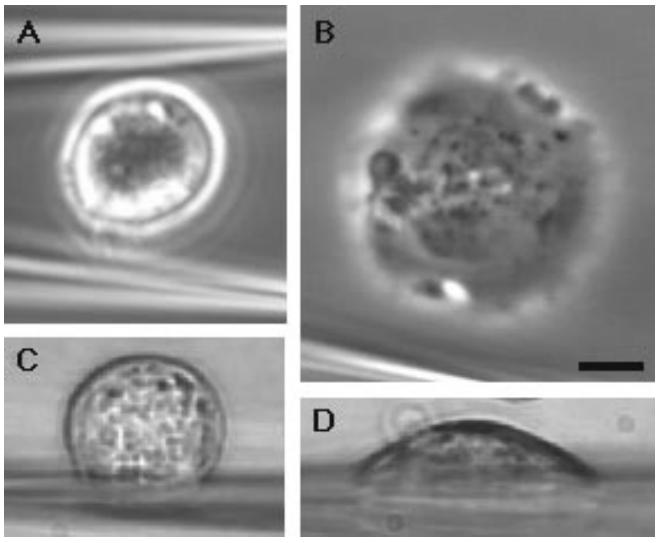

Fig. 3 A–D Adhesion and spreading of fibroblasts on microplates. The cell on the *left* has adhered on the microplate for 5 min (**A, C**). The cell on the *right* has been allowed to spread at 37 °C for 3 h (**B, D**). *Upper views* (**A, B**) are in phase contrast, *side views* (**C, D**) are in bright field. *Bar*, 5 μm

promote spreading, cells were incubated at 37 °C in the presence of serum, for up to 3 h (Fig. 3B, D). After staining with rhodamine-phalloidin, a dense cortical layer was apparent in adherent cells, whereas in spread cells F-actin was organized in a more complex fibrillar network (not shown). By rotating microplates, one could obtain both upper and side views, allowing determination of cell height, contact diameter, and contact angle (Fig. 2B). We plotted these parameters for the 70 cells examined in this study (Fig. 4). The use of contrasting conditions of spreading (from suspended cells to almost fully spread cells) allowed us to vary morphometric parameters over a large range (Table 1). As cells flatten out on microplates, the cell-microplate contact angle increases, the contact diameter increases, and the cell height decreases (Fig. 4). We could fit these data quite well with simple theoretical expressions, approximating cell shape by a truncated sphere of constant volume, which was in reasonable agreement with the images and data obtained (Fig. 3 and Table 1). This gave reference diameters R_0 between 12 μm and 16 μm, close to the size of control round cells. A significant increase in apparent surface area (up to 50%) was observed upon fibroblast adhesion and spreading (Table 1), which could be modeled using our geometric analysis (not shown).

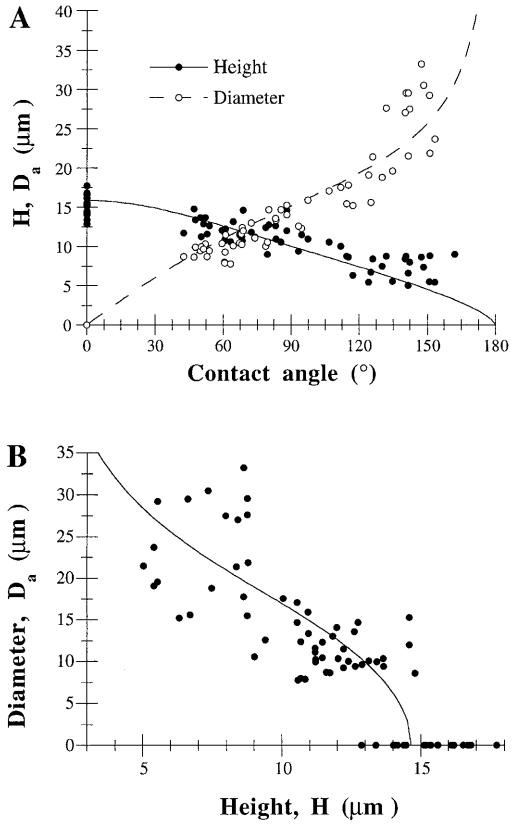

Fig. 4 A, B Morphometric changes during cell spreading. **A** The cell height (H) and the diameter of conjugation between the cell and the microplate (D_a) are shown versus the contact angle (θ_a). Each point represents one cell (n = 70). The plain curves are theoretical relationships given by Eqs. (2) and (3) in the analysis. **B** Relationship between contact diameter and cell height; the *solid curve* corresponds to Eq. (4)

Fibroblast cortical tension

To estimate their mechanical properties, fibroblasts at varying degrees of spreading were aspirated into a micropipet. Negative pressure was first increased by small increments, until the cell formed a static hemispherical cap into the pipet. No further penetration of the cell was observed if the pressure was maintained at this equilibrium value (not shown). The area of the cell aspirated at the equilibrium pressure was not significantly different from that of the non-aspirated cell (not shown). Thus, we set $\alpha = 0$ in Eq. (1), giving $\tau_0 \sim \tau_{eq}$. The persistent cortical tension was estimated from the equilibrium pressure (ΔP_{eq}) and mor-

Table 1 Morphometry of fibroblasts in different spreading conditions. Data are expressed as mean ± standard deviation. The contact angle (θ_a), cell height (H), and diameter of the contact zone (D_a) were measured directly from side-view images. Cell surface area (S) and volume (V) were computed from 3D reconstructions of cell shape

Condition	n	θ_a (°)	H (μm)	D_a (μM)	S (μm^2)	V (μm^3)
Suspended-control	16	0	15.3 ± 1.3 [a]	0	735 ± 120	1825 ± 450
Suspended-3 h	5	0	15.4 ± 1.2 [a]	0	725 ± 110	1790 ± 400
Suspended-cyt D	12	0	14.2 ± 1.6 [a]	0	640 ± 140	1550 ± 520
Adherent	16	71 ± 14	12.5 ± 1.3	11.5 ± 2.0	760 ± 130	1730 ± 430
Spread-0.5 h	15	101 ± 27	10.1 ± 1.3	17.3 ± 6.8	880 ± 400	1750 ± 680
Spread-3 h	15	134 ± 21	7.3 ± 1.4	24.4 ± 10.5	1090 ± 400	1600 ± 650

[a] The height of suspended cells was taken equal to their diameter ($H = 2R_0$)

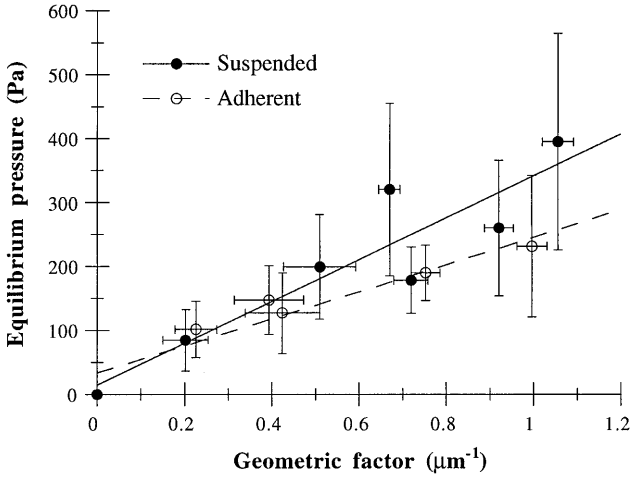

Fig. 5 Validation of the relationship between cortical tension and aspiration pressure. The micropipet diameter was varied between 3 μm and 8 μm. For each diameter, the equilibrium pressure corresponding to the formation of a hemispherical cap into the pipet was determined for 5–15 fibroblasts. The average value is plotted versus the geometric factor in Eqs. (5) and (8). The relationship is linear for both conditions, the slope of which being taken as the resting cortical tension. We found $\tau_0 = 3.3\times10^{-4}$ N/m for suspended fibroblasts ($r = 0.92$, $n = 63$ cells), and 2.1×10^{-4} N/m for adherent ones ($r = 0.96$, $n = 48$)

phometric parameters, using Eq. (5) for suspended cells and Eq. (8) for adherent cells. The validity of these two expressions was subjected to experimental test by varying the pipet diameter from 3 μm to 8 μm (Evans and Yeung 1989): this allowed the geometric factor, i.e. $2(1/R_p - 1/R_c)$ for suspended cells and $2[1/R_p - (R_a \sin\theta_a - R_p \sin\theta_p)/(R_a^2 - R_p^2)]$ for adherent cells, to vary from 0.2 μm to about 1 μm^{-1}. The relationship between ΔP_{eq} and these geometric factors was linear (Fig. 5), as predicted by the equations. Neither the equilibrium pressure nor the cortical tension were found to be significantly affected by cell spreading (Table 2); if anything, they showed a small decrease upon fibroblast adhesion and spreading (Fig. 5). However, the cortical tension of suspended cells treated with cytochalasin to perturb actin polymerization, or butanedione monoxime to inhibit myosin ATPase activity (Waterman-Storer and Salmon 1997) was decreased by respectively 44% and 21% (Table 2).

Surface elasticity of the fibroblast cortex

After the equilibrium phase, the aspiration pressure was quickly set from ΔP_{eq} to 30 mmH_2O above ΔP_{eq} for 10 min, then set back to ΔP_{eq} for another 5 min (Fig. 6). At all stages of spreading, cells exhibited a strong initial penetration into the pipet (Fig. 7A), accompanied by an increase in surface area (Fig. 7B). Furthermore, when pressure was set back to the equilibrium value, the cell showed a small recoil, manifest both in the length of the aspirated portion (10–20% decrease) and in the surface area. This overall behavior was in agreement with area elasticity of the cortex (Eq. 1). The relative change in surface area, α, was on the order of a few percent and found to decrease with spreading (Table 2). The area expansion modulus (K) calculated through Eq. (11), was around 10^{-2} N/m and found to increase by as much as 40% in the process of cell spreading, but was not affected by treatment with cytochalasin D (Table 2).

Apparent viscosity of the fibroblast interior

From the long term penetration of the cell into the pipet, one could detect viscous effects. After the initial phase, cells exhibited slow and steady penetration into the pipet (Fig. 6). When the pressure was set back to ΔP_{eq} at the end of the 10 min period, the aspirated portion did not retract much (Fig. 7A). Moreover, when cells were removed from the pipet at the end of the aspiration test, they retained a very deformed shape (Fig. 8D). Then, cells went back to their original shape in a time scale of about 10 min, owing to cortical tension (not shown). All these observations were in agreement with a viscous behavior of the cell interior. The apparent viscosity, in the range of 2–4 10^4 Pa s, was found to increase by almost a factor of 2 in the course of cell spreading, but did not change upon perturbation of actin with cytochalasin (Table 2).

Basal force

In order to validate the mechanical analysis, we measured the force exchanged between the cell and the microplate

Table 2 Mechanical parameters of fibroblasts at different stages of spreading. The persistent tension (τ_0), the area elastic modulus (K), and the apparent viscosity (μ) were determined by fitting the data with expressions described in the theoretical analysis. The equilibrium pressure (ΔP_{eq}) and the fractional area expansion (α) are also shown. Data are expressed as mean ± standard deviation

Condition	n	ΔP_{eq} (N/m^2)	τ_0 (10^{-4} N/m)	α (%)	K (10^{-2} N/m)	μ (10^4 Pa s)
Suspended-control	16	199 ± 82	3.91 ± 1.51	4.04 ± 2.47	1.62 ± 0.97	1.92 ± 0.69
Suspended-3 h	5	132 ± 76	2.80 ± 1.69	6.44 ± 1.33	0.98 ± 0.19	1.77 ± 0.79
Suspended-cyt D	12	94 ± 42	2.19 ± 1.09 [a]	5.49 ± 3.82	1.86 ± 1.82	2.14 ± 1.11
Suspended-BDM	17	139 ± 53	2.83 ± 1.02 [a]	ND [b]	ND	ND
Adherent	14	127 ± 63	2.98 ± 1.35	4.64 ± 2.59	1.90 ± 1.61	2.63 ± 1.29
Spread-0.5 h	13	146 ± 52	2.70 ± 0.94	3.76 ± 2.50	2.08 ± 1.81	2.95 ± 1.21 [c]
Spread-3 h	14	182 ± 62	3.03 ± 1.15	2.88 ± 1.96	2.23 ± 1.55	3.78 ± 2.37 [c]

[a] The cortical tension of suspended fibroblasts treated with cytochalasin D or butanedione monoxime was significantly lower than that of control cells ($P = 0.005$ and 0.05, respectively)
[b] Not determined
[c] The apparent viscosity of cells spread for 0.5 h or 3 h was significantly higher than that of suspended cells (unpaired t-test, $P = 0.02$ and 0.005, respectively)

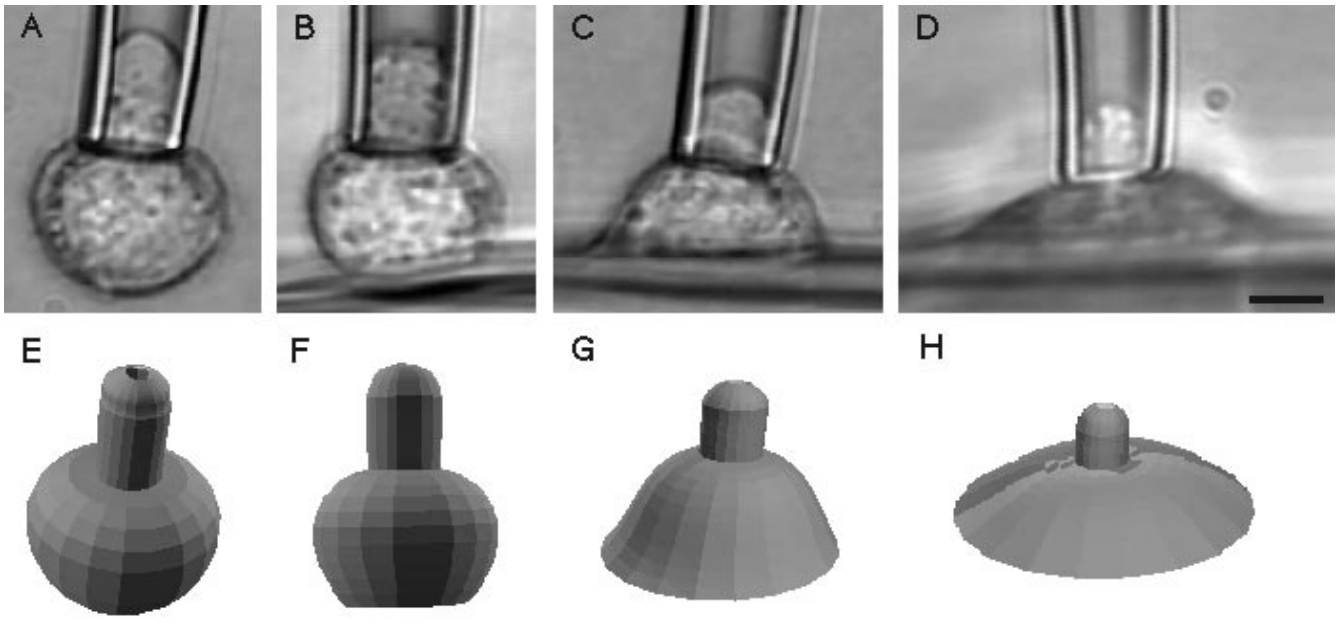

Fig. 6A–H Micropipet aspiration of fibroblasts at different stages of spreading. **A**, **E** Suspended fibroblast. **B**, **F** The cell has adhered for 5 min before aspiration. Cells were incubated at 37°C for 0.5 h (**C**, **G**) or 3 h (**D**, **H**) to promote spreading. In the upper part of the figure (**A–D**), actual cells are shown 5 min after adjustment of the aspiration pressure to 30 mmH_2O above the equilibrium value. The cell is in the middle of the image, sitting on the microplate (*bottom contour* in **B**, **C**, and **D**), and the micropipet (*cylinder*) comes from the top. In the *lower part* (**E–H**), the corresponding images are three-dimensional reconstructions of cellular shape during aspiration; the computer analysis allowed quantitation of cell area and volume. Note that penetration is lower in spread cells, relatively to suspended and adherent cells. In these experiments, the pipet diameter was 5.3±0.5 μm (mean±SD, n = 15 pipets). *Bar*, 5 μm

during micropipet aspiration of adherent cells, and compared it to the one predicted by the model. Cells were seized on flexible microplates, and exposed to the same aspiration test described above (Fig. 8). The force at the cell-microplate interface was estimated from the deflection of the microplate, after appropriate calibration. A force around 0.5 nN was already detectable when the pressure was maintained at its equilibrium value (Fig. 9). The force was found to increase rapidly to a plateau around 1.2 nN when the aspiration pressure was set to 30 mmH_2O above ΔP_{eq}, then relaxed slowly when the pressure was set back to ΔP_{eq} (Fig. 9). A theoretical force was derived from knowledge of imposed pressure and cell morphometry (Eq. 15). At the equilibrium pressure (time between –3 min and 0 min and between 10 and 15 min), the theoretical force was very close to the one measured experimentally (Fig. 9). During the aspiration phase (time between 0 min and 10 min), the predicted force was slightly higher than the measured one. This was mainly due to the fact that our calculation hypothesized mechanical equilibrium, while cells were in fact continuously deforming during this phase (part of the force imposed at the apical surface was dissipated through cell deformation, and not transmitted to the basal surface).

Discussion

Novelty of the experimental approach

In this study, we examined changes in fibroblast mechanical properties accompanying spreading. Chick fibroblasts were chosen as a model cell system because their structural, adhesive, and migratory properties are well documented (Harris 1988, 1990). In addition, we already had information on their viscoelastic and contractile properties (Thoumine and Ott 1996, 1997 a). We could accurately vary and measure the degree of fibroblast spreading on glass microplates, which have the advantage of being flat, transparent, and adhesive surfaces. Spreading was accompanied by a structural organization of the actin network similar to that reported in other studies (Sorrano and Bell 1982; David-Pfeuty 1985; Vasiliev 1985; Bereiter-Hahn et al. 1990; Mooney et al. 1995). The micromanipulation system provided excellent side views of the cells, comparable to images obtained with other techniques (Ingram 1969; Hlinka and Sanders 1972; Boocock et al. 1984; Roth et al. 1988; Tözeren et al. 1992; Cao et al. 1997). This allowed precise morphometric measurements; in particular, we could calculate cell area and volume in an axisymmetric geometry using a new computer method. Moreover, the micropipet provided a control of the pressure with an accuracy of 0.5 mmH_2O (corresponding to a force of 0.2 nN), and the microplate allowed the measurement of forces at the basal surface (in the nN range). To our knowledge, these experiments represent one of the first attempts to probe simultaneously forces at both ends of a cell and correlate them. Forces and deformations were related through a theoretical model, allowing computation of the mechanical properties of fibroblasts.

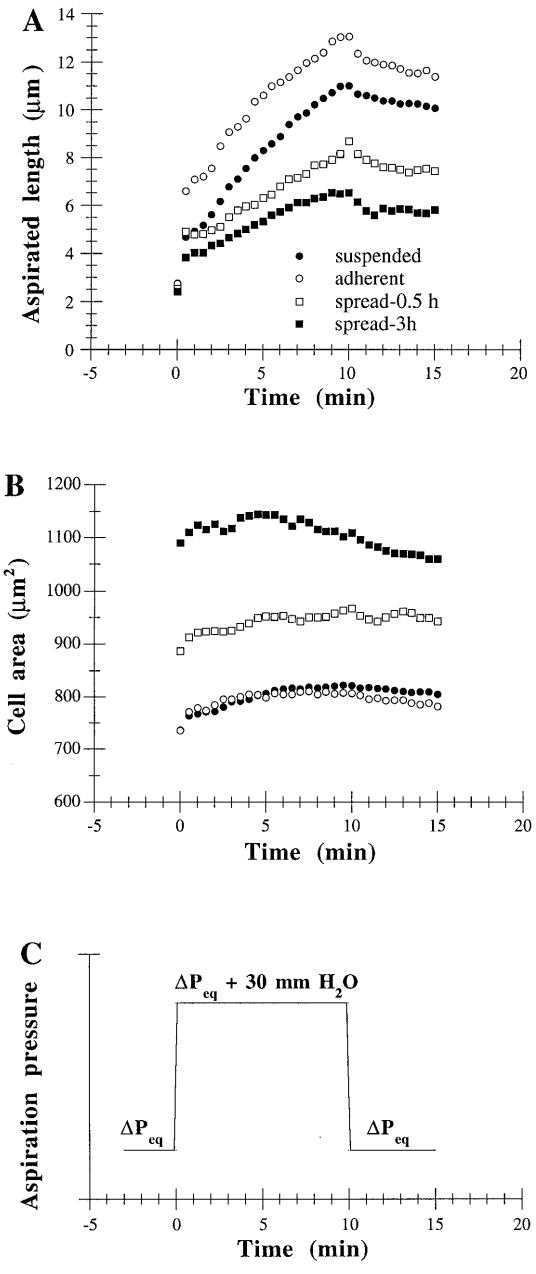

Fig. 7A–C Quantification of morphological changes during aspiration of fibroblasts. Micropipet aspiration tests were carried out on four categories of cells: (1) suspended; (2) adherent; (3) spread for 0.5 h; and (4) spread for 3 h. Two quantities are shown: **A** the length of the portion penetrating into the pipet, and **B** the overall surface area of the cells. The pressure was set as indicated in **C**: at time zero, the aspiration pressure was increased by 30 mmH_2O above the equilibrium pressure (ΔP_{eq}), and maintained constant for 10 min. It was then set back to ΔP_{eq} for 5 min. Note in plot **A** the fast initial regime, followed by a smooth linear length increase. The surface area increased slightly following the pressure jump (right after time zero), then remained fairly constant. Cell volume varied on average by 4–9% during aspiration (not shown). Each point represents an average of about 15 cells. Standard errors are 14–36% of the mean value for the length, and 13–45% for the area. Note that the apparent area increases with cell spreading

Validity of the model and measurements

Our model of the fibroblast structure is that of a fluid core bounded by a contractile cortex. The cortex was described by both persistent tension and area elasticity, and the internal fluid was characterized by a large apparent viscosity. Other models may be equally valid, but they would have to be thoroughly justified. For example, a viscoelastic model with a yield stress is not consistent with previous experiments using two microplates (Thoumine and Ott 1997a), which show a linear stress-strain relationship when cells are stretched in the elastic regime (at short term), while the tensegrity paradigm (Wang et al. 1993) does not predict the observed viscous behavior. Advantages of our model are that it is particularly suited to the axisymmetric geometry and leads to analytic expressions. Although reducing cell structural complexity to a minimal number of constituents with simple mechanical properties, this analysis described most of the fibroblast behavior in our experiments. First, it agreed with the actual shapes of adherent and spread fibroblasts, which looked like truncated spheres of constant volume. Second, it predicted that the equilibrium aspiration pressure should increase linearly with the inverse of the pipet diameter, which was tested experimentally for both suspended and adherent cells. This allowed computation of the resting cortical tension (in the range of 2–4 10^{-4} N/m). Third, the hypothesis of area elasticity was confirmed by a rapid initial entry of fibroblasts in the micropipet upon a step increase in pressure, accompanied by an increase in surface area of about 3–6%. This behavior allowed calculation of the area expansion modulus, K. Fourth, the hypothesis of a very viscous core agreed with the slow, steady and irreversible penetration of fibroblasts into the micropipet at a pressure above the equilibrium value. The viscosity found for suspended fibroblasts agrees well with a value (10^4 Pa s) calculated for the same cells using a technique of dual microplate manipulation (Thoumine and Ott 1997a). Furthermore, from knowledge of the viscosity and cortical tension, one can estimate a relaxation time: $t = \mu R_0/\tau_0$ (Tran-Son-Tay et al. 1991), where R_0 is the radius of suspended cells (a characteristic length). With average values μ=2.6×10^4 Pa s, $\tau_0 = 3\times10^{-4}$ N/m, and $R_0 = 8$ μm, one gets $t = 12$ min, which is close to the time it took cells to relax to their original shape at the end of aspiration test, pulled together by the cortical tension. These facts give credit to the approximate expressions used for computation of the viscosity. Finally, the model accurately predicted the relationship between pressure in the micropipet and force transmitted at the microplate surface, especially in the equilibrium phase. The forces detected at the basal surface, around 1 nN, are 2–3 orders of magnitude lower than those necessary to detach the cell from its substrate (Tözeren et al. 1992); indeed, we did not observe much change in the geometry of the contact zone during aspiration. However, such forces are likely to increase the cell-substrate separation distance, as demonstrated for osteoblast-like cells pulled on with magnetic microspheres (Lo et al. 1998). If the same spring constant (k = 28 pN/nm at room temperature) were to hold for fi-

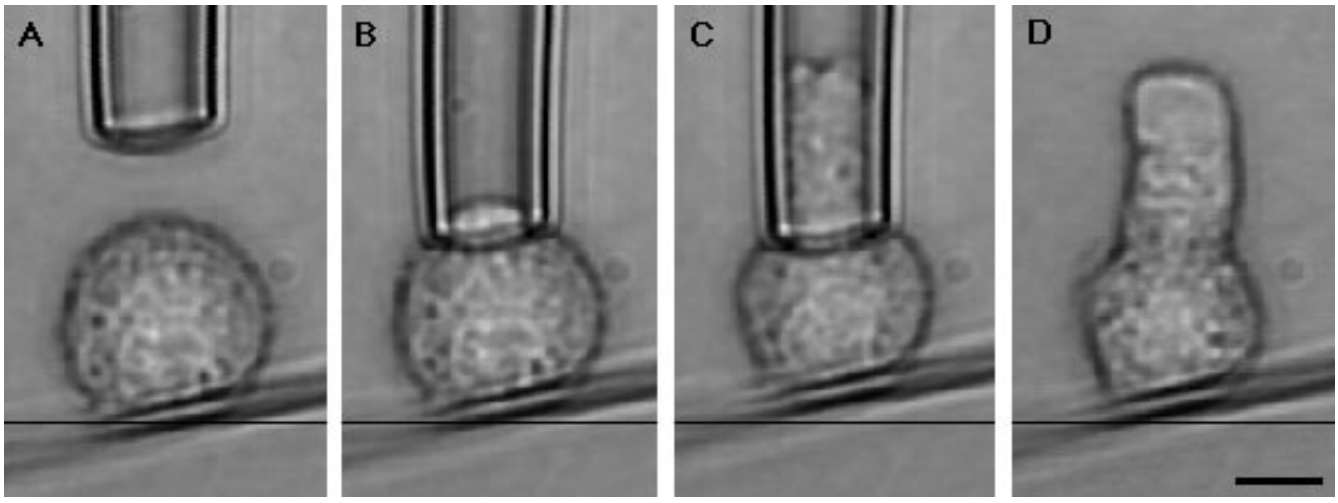

Fig. 8 A–D Micropipet aspiration of a fibroblast adherent to a flexible microplate. **A** A fibroblast (*center*) was captured on a microplate (*bottom contour*), and viewed from the side. A pipet (*top profile*) was approached and the negative pressure was raised by increments until a hemispherical cap formed in the pipet (**B**). Then, the pressure was increased by 30 mmH_2O, and aspiration proceeded for 10 min. The cell in **C** is shown after 5 min. The pressure was set back to its equilibrium value, and the cell was allowed to relax for 5 min. Finally, the micropipet was removed (**D**). Afterwards, the cell relaxed in about 10 min to its original shape, as in **A** (not shown). Note the penetration of the cell into the pipet, and the concomitant deflection of the microplate from its equilibrium position (*black horizontal line*), which ranged from about 0.2 μm to 4 μm. *Bar*, 5 μm

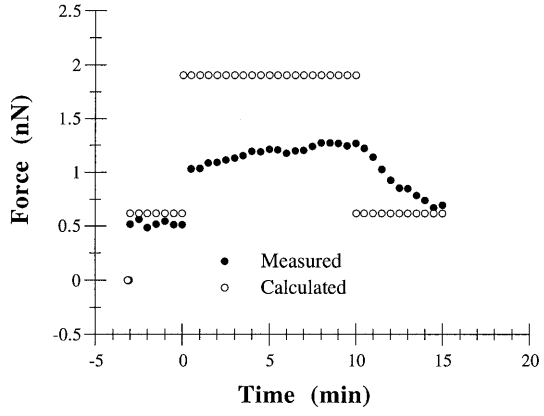

Fig. 9 Changes in basal force over time during the aspiration test. The experimental force (*solid circles*) was estimated from the deflection of the flexible microplate, after calibration. The theoretical expression (*open circles*) was calculated from knowledge of the pressure and geometry, using Eq. (15). The morphometric factors did not vary much during aspiration; they were thus measured only once, at the middle of the aspiration period. This is why the theoretical estimate is constant. Each point represents an average of 15 cells. The standard error is 54–77% of the mean value for the experimental determination, and 57–61% for the theoretical one

broblasts, one could then predict an elevation of 18–43 nm upon micropipet aspiration, which is too low to be detected by optical microscopy.

Meaning of the mechanical properties

In the model, cortical tension was attributed to an actin-rich peripheral layer, in agreement with our observations of F-actin distribution in fibroblasts (not shown). Cortical tension probably relies on an actin-myosin contraction mechanism since treatment of fibroblasts with butanedione monoxime (a known inhibitor of myosin function) or cytochalasin D at doses sufficient to cause effective depolymerization of the actin network (Thoumine and Ott 1996) both caused a decrease in τ_0. A similar drop in cortical tension has been reported for leukocytes upon treatment with cytochalasin (Tsai et al. 1994; Ting-Beall et al. 1995). Depolymerizing actin is also known to inhibit the contractility of chick fibroblasts in other experimental systems, i.e. permeabilized cells stimulated with ATP (Thoumine and Ott 1996), or cells seized between microplates (Thoumine and Ott 1997a). Occasionally, we observed the formation of vesicles at the penetrating front in cytochalasin-treated cells, confirming that the cortex had become weaker. However, we never saw separation of the membrane from the cytoplasm in untreated cells (within the limit of optical resolution): granular material was present all the way to the tip of the protrusion. This behavior is in contrast with that of red blood cells, which show a clear segregation of lipids from cytoskeletal proteins upon aspiration in a micropipet above a critical pressure (Discher et al. 1994). The difference is probably due to the fact that in fibroblasts there is excess membrane area (even in spread cells, see below), so that deformation is accompanied by unfolding of surface wrinkles, not stretching of the plasma membrane. In contrast, the surface of swollen erythrocytes is fully extended, giving rise to higher tensions and eventually separation of the membrane from its supporting cytoskeleton. Finally, we observed a large scatter in the measurements of cortical tension, which may partially be due to the fact that individual cells are not all in the same phase of their growth cycle. Future experiments on synchronized cell populations

should show if each growth phase is characterized by a specific stiffness.

Aspiration of fibroblasts into micropipets is likely to be accompanied by stretching of the actin-rich cortex. Supposedly, the volume of the cortex remains constant, and its area increases by a few percent upon aspiration (Yeung and Evans 1989). This 2D isotropic deformation was characterized by an area expansion elastic modulus, K, which was found to be quite high (around 10^{-2} N/m), suggesting it is relatively difficult to stretch the fibroblast cortex. Theoretical calculations have been made that predict the relationship between the cell-substrate contact angle (θ_a) and the dimensionless adhesive energy, w_a/τ_0, for various values of the ratio K/τ_0 (Evans 1995). In our experiments, K/τ_0 is around 30, giving $w_a/\tau_0 = 10$ for a contact angle of 90° (situation of intermediate spreading). Thus, the adhesive energy per unit area, w_a, should be around 3×10^{-3} N/m, about 10 times larger than that measured for T lymphocytes adhering to ICAM-1 (Tözeren et al. 1992) or two erythrocytes bound by agglutinins (Evans and Leung 1984). The discrepancy may be attributed to differences at several levels (cell type, adhesive molecules, extent of spreading, temperature).

If the balance between cortical tension and adhesiveness dictates the final extent of spreading for a cell, cytoplasmic viscosity is likely to affect the rate at which cells spread. The high values found here for fibroblasts are in agreement with spreading being a rather slow process. The apparent viscosity of the cell core, represented by the parameter μ, expresses overall dissipation of mechanical energy through irreversible phenomena, which can include cytosolic flow and rearrangement of the cytoskeletal network. Other processes such as depolymerization and repolymerization of filaments may also play a role. However, treatment with cytochalasin did not affect the apparent viscosity of round fibroblasts. Furthermore, no accumulation of polymerized actin was observed inside the micropipet upon aspiration of suspended cells (not shown). This suggested that actin polymerization was not necessary for cell entry in the micropipet. The cell nucleus being quite rigid (Maniotis et al. 1997; Caille et al. 1998), it may raise the apparent viscosity if it gets plugged at the micropipet mouth (Tran-Son-Tay et al. 1998). However, we never observed cessation of flow during aspiration, and stained nucleus were always found in the cellular part outside the pipet and not particularly close to the mouth (not shown), suggesting that in our experiments the nucleus does not interfere with cytoplasmic flow.

Overall, the three mechanical parameters (cortical tension, area expansion modulus, and apparent viscosity) are much larger for fibroblasts than for leukocytes (Evans and Yeung 1989; Tran-Son-Tay et al. 1991; Needham and Hochmuth 1992). These differences may be related to contrasting mechanical roles played by the two cell types: fibroblasts provide structural support to connective tissues and have to develop and resist large forces, whereas white blood cells must be soft enough to enter capillaries. It is our hope that the microplate technology can be used to further test existing models of leukocyte rheology.

Changes during spreading

Fibroblast spreading was accompanied by a 50% increase in total cell surface area, which must involve unfolding of plasma membrane wrinkles since lipid bilayers can accomodate only a few percent area increase (Evans et al. 1980). Experiments of microsphere engulfment (Simon and Schmid-Schönbein 1988) and micropipet aspiration (Evans and Yeung 1989) have shown that there is 80–100% excess membrane area in leukocytes. If the same values hold for fibroblasts, one may expect that the membrane is not totally unfolded in cells spread for 3 h. We thought that the increase in surface area upon spreading could be accompanied by stretching of the actin-rich cortex, possibly resulting in changes in mechanical properties at the fibroblast surface. We observed a slight decrease in the resting cortical tension τ_0 upon cell adhesion and spreading, more prominent for adherent cells. One explanation of this phenomenon would be that stretching of the cortex occurs upon adhesion and is accompanied by a relaxation of the outer surface (the one probed by the micropipet). Another possible mechanism is that the volume of the cortex increases during cell spreading, allowing the apparent area to rise with no change in the resting tension. In contrast, the elastic area expansion modulus K was increased in adherent and spread cells versus suspended cells, indicating that the cortex had become stiffer. The increase in surface rigidity upon spreading may be due to changes in the cell internal structure. Crosslinking of actin filaments, which is known to increase gel rigidity in purified systems (Janmey et al. 1990), might be involved in such cortical stiffening. Others studies have reported similar surface hardening upon cell restructuration. In response to fluid shear stress, endothelial cell elongation (concomitant to the formation of actin filament bundles) correlates with a large increase in surface stiffness, as probed by micropipet apiration (Sato et al. 1987). As another example, the cortical strength of endothelial cells increases with projected cell surface area, as judged by cytomagnetometry (Wang and Ingber 1994, 1995). Since transformed cells are usually less spread than their normal counterparts (Vasiliev 1985), the increase in rigidity accompanying fibroblast spreading may be related to the fact that transformed cells are more deformable than normal cells (Erickson 1980; Thoumine and Ott 1997b). Finally, the rate of penetration of fibroblasts into micropipets was lowered by spreading, giving rise to higher apparent viscosities for spread cells (3.8×10^4 Pa s) than for cells in suspension (1.9×10^4 Pa s) and adherent fibroblasts (2.6×10^4 Pa s). Endothelial cells also exhibit similar increases in internal viscosity with projected area (Wang and Ingber 1994, 1995), although the reported values are lower than ours, probably owing to the use of different cells, experimental systems, and mechanical analyses. It is known that the viscosity of actin solutions is enhanced by polymer length and degree of crosslinking (Janmey et al. 1988). The increased apparent viscosity with cell spreading may be due to such structural alterations in the cytoskeleton. Alternatively, active phenomena, e.g. polymerization of cytoskeletal filaments, may contribute to increase the ap-

parent viscosity. For example, spread cells often extended transient protrusions in the micropipet, whereas suspended cells exhibited a more steady penetration.

Conclusion

In this paper, we characterized the mechanical behavior of spreading fibroblasts: a novel micromanipulation technique coupled to a theoretical approach allowed computation of cortical tension, surface elasticity, viscosity, and force at the basal surface. The mechanical analysis described fairly well the observed cellular behavior. It is well known that perturbing the cytoskeleton, for example by drugs which inhibit filament polymerization decreases cell stiffness. Here, on the other hand, we show that structural organization promoted by spreading results in cell stiffening. The next step is to establish correlations between cytoskeletal organization underlying cell spreading and changes in rheology. Taken together, our observations provide new information on fibroblast mechanics, which play an important role in connective tissue organization and repair.

Acknowledgements This work was supported by funds from EPFL and CNRS. The authors thank D.-E. Backman, N. Caille and Y. Tardy for designing the system to transfer cells from the microscope to the incubator, A. Kottelat for expert technical assistance and help with image analysis, D. Busset for the rack-and-pinion elevation setup, and A. Ott and T. M. Quinn for critically reading the manuscript.

References

Albrecht-Buehler G (1987) Role of cortical tension in fibroblast shape and movement. Cell Motil Cytoskel 7: 54–67

Bardsley WG, Aplin JD (1983) Kinetic analysis of cell spreading. I. Theory and modeling of curves. J Cell Sci 61: 365–373

Bereiter-Hahn J, Lück M, Miebach T, Stelzer HK, Vöth M (1990) Spreading of trypsinized cells: cytoskeletal dynamics and energy requirements. J Cell Sci 96: 171–188

Boocock CA, Brown AF, Dunn GA (1984) A simple chamber for observing microscopic specimens in both top and side views. J Microsc 137: 29–34

Caille N, Tardy Y, Meister JJ (1998) Assessment of strain field in endothelial cells subjected to uniaxial deformation of their substrate. Ann Biomed Eng 26: 409–416

Cao J, Usami S, Dong C (1997) Development of a side-view chamber for studying cell-surface adhesion under flow conditions. Ann Biomed Eng 25: 573–580

Chicurel ME, Chen CS, Ingber DE (1998) Cellular control lies in the balance of forces. Curr Opin Cell Biol 10: 232–239

Choquet D, Felsenfeld DP, Sheetz MP (1997) Extracellular matrix rigidity causes strengthening of integrin-cytoskeletal linkages. Cell 88: 39–48

Cramer LP, Mitchison TJ, Theriot JA (1994) Actin-dependent motile forces and cell motility. Curr Opin Cell Biol 6: 82–86

David-Pfeuty T (1985) The coordinate organization of vinculin and of actin filaments during the early stages of fibroblast spreading on a substratum. Eur J Cell Biol 36: 195–200

Dennerll T, Lamoureux P, Buxbaum RE, Heidemann SR (1989) The cytomechanics of axonal elongation and retraction. J Cell Biol 109: 3073–3083

Discher DE, Mohandas N, Evans EA (1994) Molecular maps of red cell deformation: hidden elasticity and in situ connectivity. Science 266: 1032–1035

Dogterom M, Yurke B (1997) Measurement of the force-velocity relation for growing microtubules. Science 278: 856–860

Dunn GA, Zicha D (1995) Dynamics of fibroblast spreading. J Cell Sci 108: 1239–1249

Elson EL (1988) Cellular mechanics as an indicator of cytoskeletal structure and function. Annu Rev Biophys Biophys Chem 17: 397–430

Erickson CA (1980) The deformability of BHK cells and polyoma visus-transformed BHK cells in relation to locomotory behavior. J Cell Sci 44: 187–200

Evans EA (1988) In: Bongrand P (ed) Physical basis of cell-cell adhesion. CRC Press, Boca Raton, pp 91–123

Evans E (1995) Physical actions in biological adhesion. In: Lipowsky R, Sackmann E (eds) Handbook of biological physics series, vol 1b. Structure and dynamics of membranes. Elsevier, Amsterdam, pp 723–754

Evans E, Leung A (1984) Adhesivity and rigidity of erythrocyte membrane in relation to wheat germ agglutinin binding. J Cell Biol 98: 1201–1208

Evans EA, Yeung A (1989) Apparent viscosity and cortical tension of blood granulocytes determined by micropipet aspiration. Biophys J 56: 151–160

Evans EA, Kwok R, McCown T (1980) Calibration of beam deflection produced by cellular forces in the 10^{-9}–10^{-6} gram range. Cell Biophys 2: 99–112

Felder S, Elson EL (1990) Mechanics of fibroblast locomotion: quantitative analysis of forces and motions at the leading lamellas of fibroblasts. J Cell Biol 111: 2513–2526

Galbraith CG, Sheetz MP (1997) A micromachined device provides a new bend on fibroblast traction forces. Proc Natl Acad Sci USA 94: 9114–9118

Harris AK (1988) Fibroblasts and myofibroblasts. Methods Enzymal 163: 623–642

Harris AK (1990) Protrusive activity of the cell surface and the movements of tissue cells. In: Akkas N (ed) Biomechanics of active movement and deformation of cells. (NATO ASI series, vol H42) Springer, Berlin Heidelberg New York, pp 249–294

Hlinka J, Sanders FK (1972) Real and reflected images of cells in profile. I. A method for the study of cell movement and adhesion. J Cell Sci 11: 221–231

Ingber D (1991) Integrins as mechanochemical transducers. Curr Opin Cell Biol 3: 841–848

Ingram VM (1969) A side view of moving fibroblasts. Nature 222: 641–644

James DW, Taylor JF (1969) The stress developed by sheets of chick fibroblasts in vitro. Exp Cell Res 54: 107–110

Janmey PA, Hvidt S, Peetermans J, Lamb J, Ferry JD, Stossel TP (1988) Viscoelasticity of F-actin and F-actin/gelsolin complexes. Biochemistry 27: 8218–8227

Janmey PA, Hvidt S, Lamb J, Stossel TP (1990) Resemblance of actin-binding protein/actin gels to covalently crosslinked networks. Nature 345: 89–92

Kolega J (1986) Effects of mechanical tension on protrusive activity and microfilament and intermediate filament organization in an epidermal epithelium moving in culture. J Cell Biol 102: 1400–1411

Kucik DF, Kuo SC, Elson EL, Sheetz MP (1991) Preferential attachment of membrane glycoproteins to the cytoskeleton at the leading edge of lamella. J Cell Biol 114: 1029–1036

Lauffenburger DA, Horwitz AF (1996) Cell migration: a physically integrated molecular process. Cell 84: 359–369

Lo CM, Glogauer M, Rossi M, Ferrier J (1998) Cell-substrate separation: effect of applied force and temperature. Eur Biophys J 27: 9–17

Maniotis AJ, Chien CS, Ingber DE (1997) Demonstration of mechanical connections between integrins, cytoskeletal filaments, and nucleoplasm that stabilize nuclear structure. Proc Natl Acad Sci USA 94: 849–854

Mooney DJ, Langer R, Ingber DE (1995) Cytoskeletal filament assembly and the control of cell spreading and function by extracellular matrix. J Cell Sci 108: 2311–2320

Needham D, Hochmuth RM (1992) A sensitive measure of surface stress in the resting neutrophil. Biophys J 61: 1664–1670

O'Neill CO, Jordan P, Ireland G (1986) Evidence for two distinct mechanisms of anchorage stimulation in freshly explanted and 3T3 swiss mouse fibroblasts. Cell 44: 489–496

Peskin CS, Odell GM, Oster GF (1993) Cellular motions and thermal fluctuations: the brownian ratchet. Biophys J 65: 316–324

Petersen NO, Mcconnaughey WB, Elson EL (1982) Dependence of locally measured cellular deformability on position on the cell, temperature, and cytochalasin b. Proc Natl Acad Sci USA 79: 5327–5331

Roth KE, Rieder CL, Bowser SS (1988) Flexible substratum technique for viewing cells from the side: some in vivo properties of primary (9+0) cilia in cultured kidney epithelia. J Cell Sci 89: 457–466

Sato M, Levesque MJ, Nerem RM (1987) Micropipette aspiration of cultured bovine aortic endothelial cells exposed to shear stress. Arteriosclerosis 7: 276–286

Schiro JA, Chan BMC, Roswit WT, Kassner PD, Pentland AP, Hemler ME, Elsen AZ, Kupper TS (1991) Integrin $\alpha_2\beta_1$ (vla-2) mediates reorganization and contraction of collagen matrices by human cells. Cell 67: 403–410

Simon SI, Schmid-Schönbein GW (1988) Biophysical aspects of microsphere engulfment by human neutrophils. Biophys J 53: 163–173

Sims JR, Karp S, Ingber DE (1992) Altering the cellular mechanical force balance results in integrated changes in cell, cytoskeletal and nuclear shape. J Cell Sci 103: 1215–1222

Soranno T, Bell E (1982) Cytostructural dynamics and spreading of translocating cells. J Cell Biol 95: 127–136

Stopak D, Harris AK (1982) Connective tissue morphogenesis by fibroblast traction. I. Tissue culture observations. Dev Biol 90: 383–398

Thoumine O, Ott A (1996) Influence of adhesion and cytoskeletal integrity on fibroblast traction. Cell Motil Cytoskel 35: 269–280

Thoumine O, Ott A (1997a) Time scale dependent viscoelastic and contractile regimes in fibroblasts probed by microplate manipulation. J Cell Sci 110: 2109–2116

Thoumine O, Ott A (1997b) Comparison of the mechanical properties of normal and transformed fibroblasts. Biorheology 34: 309–326

Ting-Beall HP, Lee AS, Hochmuth RM (1995) Effect of cytochalasin D on the mechanical properties and morphology of passive human neutrophils. Ann Biomed Eng 23: 666–671

Tözeren A, Mackie LH, Lawrence MB, Chan P-Y, Dustin ML, Springer T (1992) Micromanipulation of adhesion of phorbol 12-myristate-13-acetate-stimulated T lymphocytes to planar membranes containing intercellular adhesion molecule-1. Biophys J 63: 247–258

Tran-Son-Tay R, Needham D, Teung A, Hochmuth RM (1991) Time-dependent recovery of passive neutrophils after large deformation. Biophys J 60: 856–866

Tran-Son-Tay R, Kan HC, Udaykumar HS, Damay E, Shyy W (1998) Rheological modelling of leukocytes. Med Biol Eng Comp 36: 246–250

Tsai MA, Frank RS, Waugh RE (1994) Passive mechanical behavior of human neutrophils: effect of cytochalasin B. Biophys J 66: 2166–2172

Valberg PA, Albertini DF (1985) Cytoplasmic motions, rheology, and structure probed by a novel magnetic particle method. J Cell Biol 101: 130–140

Vasiliev JM (1985) Spreading of non-transformed and transformed cells. Biochim Biophys Acta 780: 21–65

Wang N, Ingber DE (1994) Control of cytoskeletal mechanics by extracellular matrix, cell shape and mechanical tension. Biophys J 66: 2181–2189

Wang N, Ingber DE (1995) Probing transmembrane mechanical coupling and cytomechanics using magnetic twisting cytometry. Biochem Cell Biol 73: 327–335

Wang N, Butler JP, Ingber DE (1993) Mechanotransduction across the cell surface and through the cytoskeleton. Science 260: 1124–1127

Waterman-Storer CM, Salmon ED (1997) Actomyosin-based retrograde flow of microtubules in the lamella of migrating epithelial cells influences microtubule dynamic instability and turnover and is associated with microtubule breakage and treadmilling. J Cell Biol 139: 417–434

Yanai M, Kenyon CM, Butler JP, Macklem PT, Kelly SM (1996) Intracellular pressure is a motive force for cell motion in amoeba proteus. Cell Motil Cytoskel 33: 22–29

Yeung A, Evans E (1989) Cortical shell-liquid core model for passive flow of liquid-like spherical cells into micropipets. Biophys J 56: 139–149

Zhelev DV, Hochmuth RM (1994) Human neutrophils under mechanical stress. In: Mow VC, Guilak F, Tran-Son-Tay R, Hochmuth RM (eds) Cell mechanics and cellular engineering. Springer, Berlin Heidelberg New York, pp 3–20

Zheng J, Buxbaum RE, Heidemann SR (1993) Investigation of microtubule assembly and organization accompanying tension-induced neurite initiation. J Cell Sci 104: 1239–1250